CHAPTER 4

DESIGN AND SIMULATION STUDY OF GRID-LESS RELTRON*

*Part of this work was published as:

Prabhakar Tripathi, A. Kumar, S. Dwivedi, and Pradip Kumar Jain, "Design and Simulation of the Thermionic Emission-Based Reltron Oscillator," *IEEE Transactions on Plasma Science, vol. 48, no. 2, pp. 438–445, Feb. 2020, DOI: 10.1109/TPS.2020.2966408*

CHAPTER 4

DESIGN AND SIMULATION STUDY OF GRID-LESS RELTRON

4.1. Overview

In this chapter, the design and simulation study of a highly efficient grid-less reltron using thermionic emissive cathode has been described. The grid-less reltron's detailed design process is first explained and then its RF interaction cavity is modeled with the help of commercial code "CST Studio Suite". The electromagnetic behavior of the modeled RF interaction cavity has been investigated with the help of the eigenmode solver and frequency-domain solver. In addition, a comprehensive simulation study has been performed to find out the structural dependency of the RF interaction cavity on the fundamental resonating mode frequency. The device is modeled and simulated using a particle-in-cell (PIC) solver to know its RF behavior. An electrical parametric analysis has been performed to evaluate the RF performance of the modeled device. The results obtained from the simulation show that the device is capable of producing 22 MW RF output power with a pulse width of 5 μs and device efficiency of 44%. For validation, the simulated results have been compared with the previously reported experimental results, and it has been found that the results are in agreement within 5%, indicating a good agreement with the reported experimental results.

4.2. Introduction

The HPM sources are often based on explosive emission cathodes for a high-density electron beam, and these explosive emission cathodes help in the formation of a high-density plasma in the device, due to which these sources are suffered from some inherent problems, such as

pulse shortening and low PRR [Miller *et al.* (1998)]. This creates a natural barrier to producing RF pulsed widths of more than 50–70 ns in such HPM sources.

Reltron is a promising HPM source and is mainly classified into two categories: (i) gridded reltron or explosive emission-based reltron, and (ii) grid-less reltron or thermionic emission-based reltron [Miller *et al.* (1995)]. In the case of gridded reltron, emitted electrons density is very high due to which the self-magnetic fields generated and these self-generated magnetic fields are sufficient to focus the electron beam therefore it does not require any external DC magnetic field for its operation [Miller *et al.* (1992)]. In the case of grid-less reltron, the emitted electrons density is not high enough to produce the self-magnetic field, therefore it requires a low external DC magnetic field to focus the electron beam [Miller *et al.* (1995)]. The operation mode of the device is TM_{01} mode while the RF output power is extracted through a rectangular extraction cavity in the TE_{10} mode. This inbuilt mode converter feature makes the device more efficient and simple [Miller *et al.* (1992)].

The device based on a very high-density electron beam is inherently suffered from a pulse shortening problem due to the plasma formation [Miller *et al.* (1998)]. The plasma formation occurred inside the device where high-density electrons terminate at its surface, under the condition that their front surface dose becomes >100 J/g. After such electrons strike, X-rays are generated which further helps in the plasma formation throughout the device [Kenyon (1992)]. The cathode and anode plasmas can move radially and axially, which alters the diode impedance as a result, gap closure is noticed in the device [Kim *et al.* (2009)]. This plasma disrupts the coupling between the RF waves and the electron beam in the RF interaction cavity. A high-density electron beam is generated from the cathode

and its density gets further increased after beam-wave interaction. The plasma generated in the device also limits the repetitive and long-pulsed operation of the device [Miller *et al.* (1998), Kim *et al.* (2009)]. In the grid-less reltron, for electron beam thermionic emissive cathode is used, therefore the plasma density is lower due to lower current and remains in its super-conducting zone. Hence, long-lived, longer pulse operation with a higher PRR becomes feasible [Miller *et al.* (1995)]. The impact of high energy with high repetition RF pulse on the electronic devices is more lethal than the single-shot or low repetition of the high power RF pulse. A lot of research activity on single-shot or low repetition RF power is reported from the last few decades but there is a huge research gap that is noticed on high energy, high PRR based devices.

Therefore in this chapter, design methodology, analysis, and a comprehensive simulation study of the grid-less reltron source which has a longer life, longer pulse width, and higher pulse PRR has been investigated. A complete simulation study (i.e. cold simulation and hot simulation) of the grid-less reltron oscillator is presented. Also, the effect of the different structural parameters of the SCC on the resonating frequency and the effect of different beam parameters and the post-acceleration voltage on the RF behavior of the device has been investigated through simulation.

4.3. Design Methodology

The typical schematic view of the reltron device is shown in Fig. 4.1. Fig. 4.1 (a) shows the 3D schematic view of grid-less reltron while Fig 4.1 (b) shows its RF interaction cavity. The design process of the reltron includes the desired oscillation frequency, the electron beam parameter, the operating mode of the RF interaction cavity, and ultimately the desired mode for extraction at which RF output power to be extracted.

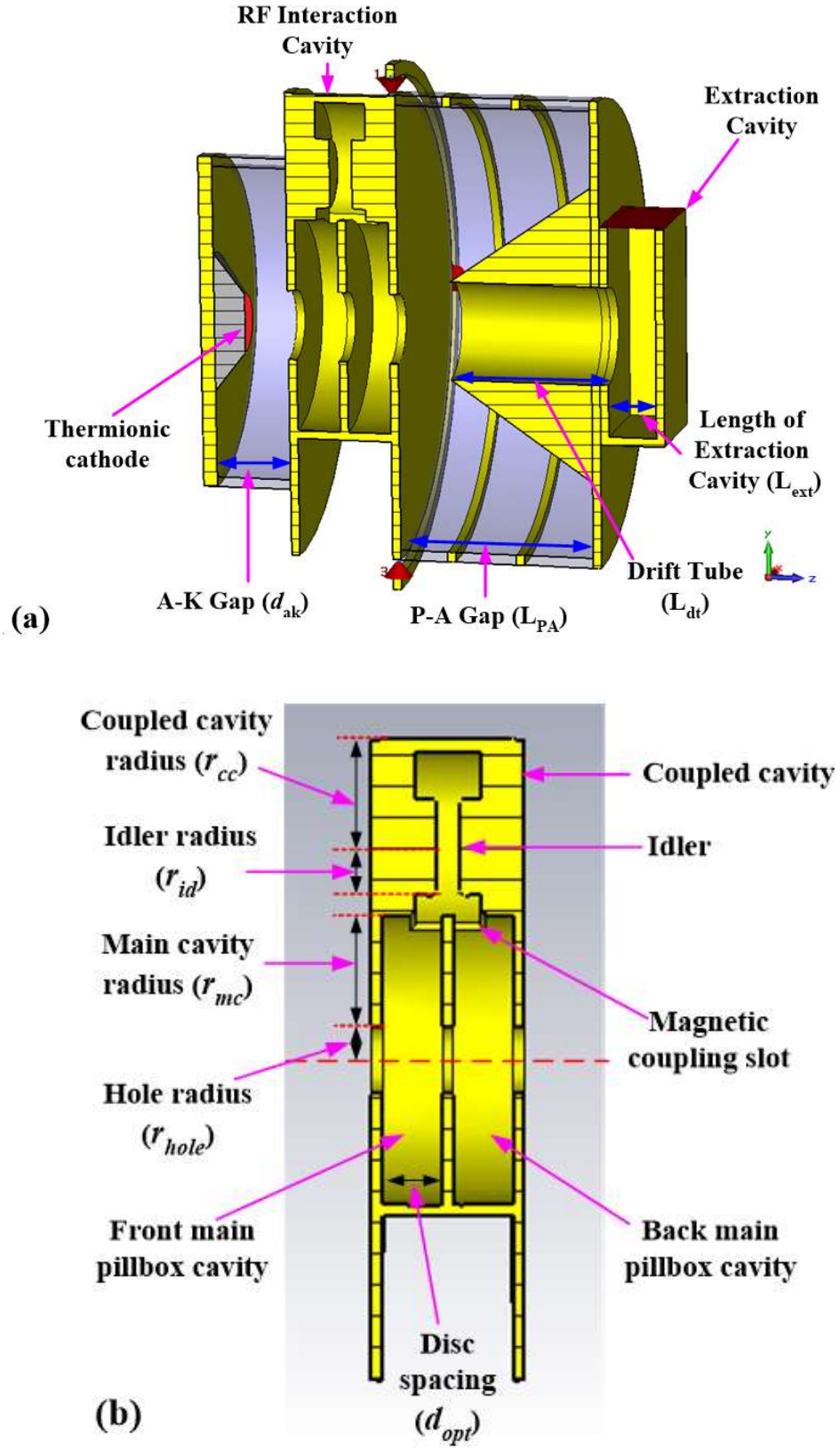

Figure 4.1: A typical reltron oscillator: (a) 3D schematic, and (b) RF interaction cavity.

The RF interaction cavity of the reltron system typically works on TM_{01} mode, and the eigenvalue for the TM_{01} mode is 2.405 for the circular waveguide. Now the desired oscillation frequency which mainly depends on the value of the main cavity radius (i.e. r_{mc}), can be determined as [Miller *et al.* (1992)]:

$$r_{mc} = \frac{\chi_{mn} c}{2\pi f_r} \tag{4.1}$$

where ' χ_{mn} ' is an eigenvalue of the cylindrical waveguiding system, ' c ' is a speed of light, and ' f_r ' is the desired operating frequency.

Since the capacitance between two parallel plates is directly proportional to its area (for circular plates, square of its radii, (i.e. r^2)), the capacitance of the coupled cavity $\left(C_0\right)$ can also be related as follows:

$$C_0 \propto r_{cc}^2 \tag{4.2}$$

From the equivalent circuit theory, the capacitance per unit length of the main pillbox cavity becomes twice the coupled-cavity capacitance. Hence, reltron main cavity capacitance $\left(2C_0\right)$ becomes proportional to its radius [Soh *et al.* (2010)]:

$$2C_0 \propto r_{mc}^2 \tag{4.3}$$

Equating expression (4.2) and (4.3), we get:

$$r_{cc} = \sqrt{2r_{mc}} \tag{4.4}$$

The idler used in the coupled cavity acts as a capacitive tuner. By varying the position of the idler, we alter the amount of coupling, which is present between the coupled cavity and the main pillbox cavity. Due to which the resonant frequency of the RF interaction cavity

changed. The isolation between the resonating modes can be increased or decreased with the help of these idlers. Miller *et al.* suggest that the radius of the idler $\left(r_{id}\right)$ can safely be taken as follows [Miller *et al.* (1992)]:

$$r_{id} \approx \frac{r_{cc}}{2} \tag{4.5}$$

In general, the disc hole radius (i.e. for electron passage) is selected as follows:

$$r_h \leq \left(r_{mc} - \frac{\lambda}{4} \right) \tag{4.6}$$

where $v\left(=v_e\right)$ is the velocity of the RF wave and needs to be synchronized with the velocity of the electron beam $\left(v_e\right)$. Here, $\lambda\left(=\lambda_e = v/f_r\right)$ is the RF wavelength, and cavity depth is taken as quarter-wavelength $\left(\lambda/4\right)$ [Dixit *et al.* (2017)]. However, based on the experimental findings, the optimum resonating cavity length is suggested as follows [Miller *et al.* (1992)]:

$$d_{opt} = \frac{v_e}{3.2 f_r} \tag{4.7}$$

Miller *et al*. performed a series of experiments to get stable and maximum power at the output in the device and found that the best choice for the anode-cathode gap $\left(d_{AK}\right)$, is about 1.1 times greater than the optimal disk spacing $\left(d_{opt}\right)$ that is [Miller *et al.* (1992)]:

$$d_{AK} = 1.1 \times d_{opt} \tag{4.8}$$

In the reltron's drift tube, both types of space charge wave will propagate, i.e. forward wave (wave associated with the positive group velocity) and the backward wave (wave associated with the negative group velocity). Since the backward propagating wave

disturbs the axial electron bunching, the radius of the drift tube of the reltron is always kept larger than the radius of the hole [Miller *et al.* (1992)]. Also, the length of the drift tube $\left(L_{dt}\right)$ is kept long so that the backward propagating wave attenuates itself within a few wavelengths. The region between the RF interaction cavity and extraction cavity is called as post-acceleration region $\left(L_{PA}\right)$ and the length of the post-acceleration region is obtained as follows [Soh *et al.* (2012), Mahto and Jain (2016)]:

$$L_{PA} = L_{dt} + L_{ext} \tag{4.9}$$

where L_{ext} is an axial length of the extraction cavity, $L_{dt} = \left(n\pi / k_z\right)$ is the length of the drift tube, and $k_z \left(= 2\pi/\lambda\right)$ is a wavenumber. For the maximum power extraction, $n\left(= 3/2, 5/2, 7/2, \ldots.\right)$ is the peaks of the current density that occurred at the center of the extraction cavity [Soh *et al.* (2012), Mahto and Jain (2016)]. Finally, the RF output power is extracted from the electron bunches at the extractor section.

Miller *et al.* assert that the diameter of the planar cathode (i.e. beam diameter of disc hole diameter) used in reltron for generating the electron beam must be nearly equal to the product of $2r_{mc}f_r^{-1}$, which also satisfies expression (4.6) [Miller *et al.* (1992)]. Miller *et al.* used a high current density thermionic cathode to obtain the electron beam current of 200 A with the current density of 4 A/cm^2 [Miller *et al.* (1995)]. For such a high current density thermionic cathode generally, Scandate, Lanthanum Hexaboride (LaB_6), or Cerium Hexaboride (CeB_6) is used as cathode materials [Cahill and Graeve (1997)]. To fulfill the desired current density (i.e. 4 A/cm^2) the required radius of the spherical pierce gun has 30.0 mm, and the electron beam radius $\left(r_e\right)$ of 11.60 mm has been taken.

To ensure the propagation of the electron beams in the grid-less reltron oscillator a small external DC magnetic field is required, which can be provided with the help of permanent magnets [Miller *et al.* (1995)]. Practically, for the confined flow of the electron beam, the magnetic field should be more than 2 to 3 times the Brillouin magnetic field and the Brillouin magnetic field calculated as [Smith and Phillips (1995), Basu (1995)]:

$$B_z^* = \sqrt{\left(0.69\times10^{-6}\right)\left(I_e \Big/ \left(\sqrt{V_e}\right) r_e^2\right)} \quad \text{Tesla.} \qquad (4.10)$$

where, I_e , V_e and r_e are the initial beam current, applied beam voltage, and radius of electron beam respectively. Generally, the radius of the electron beam is kept a little smaller than the disc hole radius to avoid the collision.

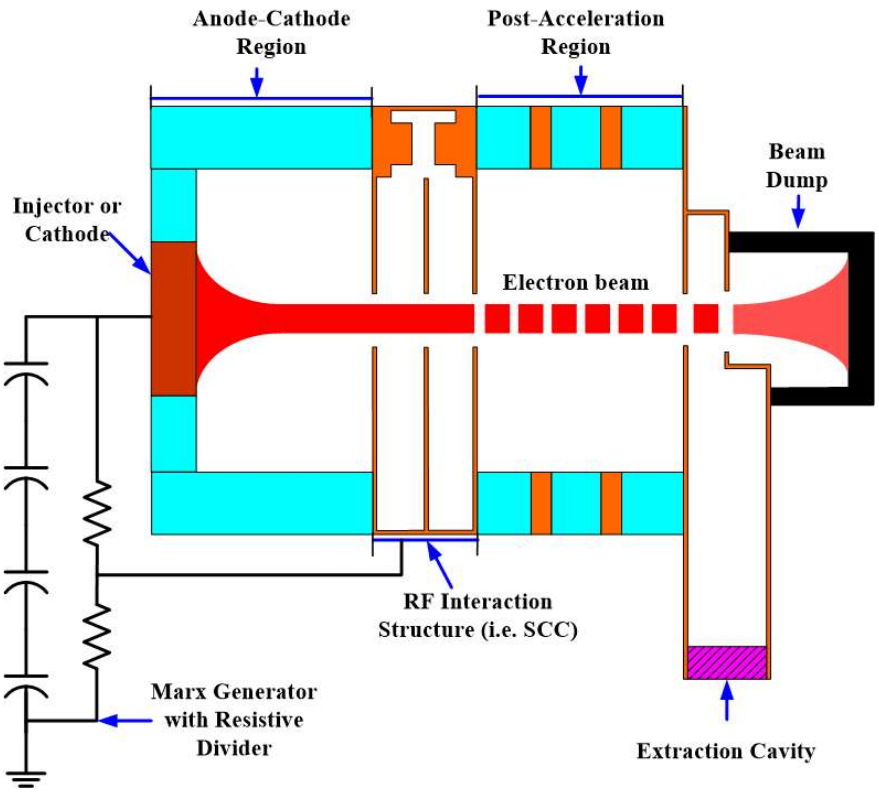

Figure 4.2: A typical schematic of the reltron oscillator.

4.4. Working Principle

The typical schematic of grid-less reltron oscillator system which is shown in Fig. 4.2, mainly consists of a high voltage pulser (i.e. Marx generator) with resistive voltage divider circuit, thermionic emissive cathode, RF interaction cavity (i.e. SCC), post-acceleration region, RF extraction cavity (i.e. rectangular extraction cavity) and collector section [Miller *et al.* (1992)].

For a high voltage DC pulse, a conventional Marx generator with a crowbar switch is used for a single pulse while for the repetitive pulse operation up to a few tens of Hertz PFN Marx pulsers is used. For applications requiring repetition rates of more than a few tens of Hertz, thyratron-switched, transformer-based systems are used. Titan has also developed a high-average-power, system capable of very high pulse repetition rates [Miller (1997)].

In grid-less reltron, the thermionic emissive cathode such as scandate cathode, or lanthanum hexaboride (LaB_6) cathode or cerium hexaboride (CeB_6) cathode is used to generate high current density electron beam. As compared to explosive emissive cathode the thermionic emissive cathode has various advantages such as long-lived, copious electron beam generation, and the probability of plasma formation is less due to which longer pulse operation with a higher PRR becomes feasible [Miller *et al.* (1995)].

The RF interaction cavity operates in the TM_{01} mode. The geometry of the RF interaction cavity consists of the main pillbox cavity, coupled-cavity, and three metal discs. These metal discs are placed at the front, middle, and end of the RF interaction cavity. The metal disc placed in the middle of the main pillbox cavity divides the cavity into two identical

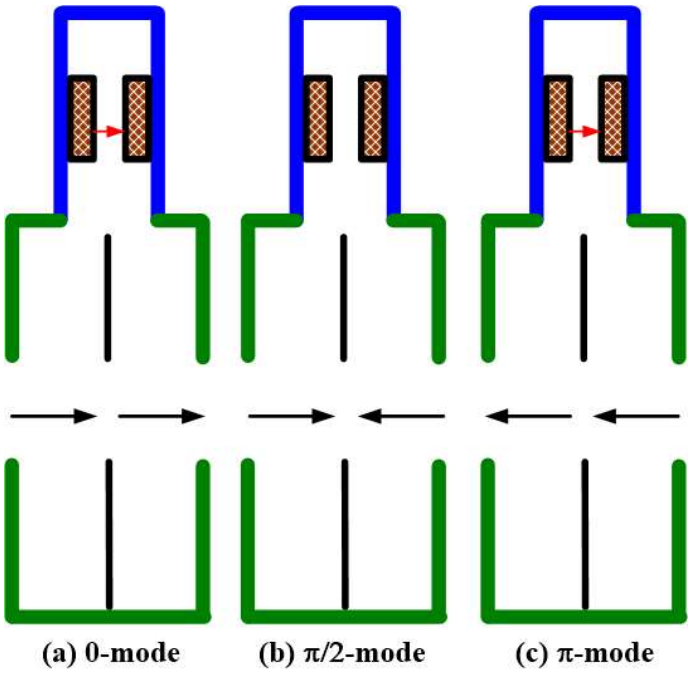

Figure 4.3: RF electric field distribution in the RF interaction cavity: (a) 0-mode. (b) π/2-mode, and (c) π-mode.

sections called front and back main pillbox cavities, respectively, as shown in Fig. 4.1 (b). The main function of the coupled cavity, which is radially connected to the main The metal disc placed in the middle of the main pillbox cavity divides the cavity into two identical sections called front and back main pillbox cavities, respectively, as shown in Fig. 4.1 (b). The main function of the coupled cavity, which is radially connected to the main pillbox cavity in the geometry, is to provide magnetic coupling between these two adjacent main pillbox cavities. This multi-cavity RF interaction resonates at three modes i.e. 0-mode, π/2-mode, and π-mode. The electric field distribution associated with these modes is shown in Fig. 4.3. For 0-mode, the electric field in both the adjacent main cavities and the coupled cavity is in the same phase i.e. the phase difference between the electric field present in the coupled cavity and the main pillbox cavities is zero which is shown in Fig. 4.3 (a), while in the case of π-mode, the electric field in the adjacent main cavities is in the same phase

but in the coupled cavity it is 180° out of phase (i.e. the phase difference between the electric field present in the coupled cavity and the main pillbox cavities is 180°) which is shown in Fig. 4.3 (c). Fig. 4.3 (b) shows the electric field distribution for the π/2-mode, which is the desired mode, where the electric field in the coupled cavity is almost zero while the electric field present in the adjacent main pillbox cavities are 180° out of phase. Initially, all three modes are excited inside the RF interaction cavity, but among them, only the π/2 mode grows because it is the only unstable mode, and it interacts with the electron beam unstably. As a result, a high degree of current modulation is achieved over a short distance [Knapp *et al.* (1965), Knapp *et al.* (1968), Miller *et al.* (1992)].

The electrons emitted from the cathode when pass through the RF interaction cavity then they encounter an accelerating and retarding electric field twice in one complete RF cycle. This accelerating and retarding RF electric field leads to a double velocity modulation, resulting in the formation of an axial electron bunch. The region of post-acceleration starts just after the RF interaction cavity and ends before the extraction cavity. The post-acceleration is an arrangement of the stacks of alternating plastic insulator rings and aluminum grading rings which act as a high voltage insulator. A hollow cone is attached to the extraction side which is used to shape the electric field in this region thereby reducing the electric field enhancement (Fig. 4.1 (a)) [Miller (1996), Soh (2012)]. A high voltage DC pulse is applied in this region, which accelerates the leaving electron bunches at relativistic speed. Due to the relativistic speed, the electrons bunch temporarily freezes, which reduces the relative kinetic spread of the electrons in the bunched beam. This post-acceleration region provides higher beam kinetic energy, which will result in more energy available at the extraction cavity. This high kinetic energy of the electron bunches is converted into RF energy with the help of a single or multiple rectangular extraction cavity

[Miller *et al.* (1992)].

The extractor section is a standard rectangular waveguide i.e. WR-284 which operates in the range of 2.60 to 3.95GHz. The RF energy is extracted in its dominant mode i.e. TE_{10} mode. The beam wave interaction in the RF interaction cavity is in TM_{01} mode, while the RF energy is extracted directly in TE_{10} mode, indicating the inbuilt mode converter which is an attractive feature of the device and also enhances the efficiency of the device. The kinetic energy of electrons is very high and is not completely converted to RF energy through a single extraction cavity so many extraction cavities can also be used to enhance the efficiency of the device [Marder *et al.* (1992), Miller *et al.* (1992)].

4.5. Simulation Study of Grid-Less Reltron

Simulation studies are essential to understand and visualize the interaction mechanism present between the electron beam and RF waves in the grid-less reltron. To achieve this goal, first of all, we designed the reltron system according to the structural specification listed in Table 4.2 and then simulated it using the commercial simulation tool "CST Studio Suite". The designed RF interaction cavity is simulated using CST's eigenmode solver and frequency domain solver (i.e. beam absent simulation) to ensure the electric field profile of the resonating mode and resonating frequency of the RF interaction cavity. Furthermore, to evaluate the device performances such as generated RF output power, efficiency, and operating frequency, the device is simulated using the CST PIC solver. For simulation, a typical S-band reltron device's electrical specification is listed in Table 4.1 is designed in CST. To validate our device design methodology described in the design methodology section, the obtained device structural parameters are listed in Table 4.2.

Table 4.1: Electrical specification of S-band grid-less reltron [Miller *et al.* (1995)].

Electrical specification	
Total tube voltage (V_{tube})	250 kV
Total beam current (I_e)	200 A
Total Beam voltage (V_e)	100 kV
Total Post-acceleration voltage (V_{PA})	150 kV

Table 4.2: Structural specification of S-band grid-less reltron [Miller *et al.* (1995)].

Structural specification	
Desired operating frequency (f_r)	2.856 GHz
Main cavity radius (r_{mc})	39.00 mm
Coupled cavity radius (r_{cc})	26.00 mm
Idler radius (r_{id})	13.00 mm
Idler length (L_{id})	5.850 mm
Disc hole radius (r_h)	12.60 mm
Disc spacing (d_{opt})	16.50 mm
Anode-cathode separation (d_{AK})	18.15 mm
Drift tube length (d_{dt})	39.00 mm
Extraction cavity length (L_{ext})	18.00 mm
Post-acceleration gap length (L_{PA})	48.00 mm
External Magnetic field (B_z^*)	0.38 Tesla

4.5.1. Cold Test Simulation Results

For the cold test simulation study (i.e. EM behavior in the absence of electron beam), the RF interaction cavity of the grid-less reltron is designed and simulated with the help of a commercial simulation tool i.e. “CST Studio Suite”. To ensure the electric field profile,

resonating frequency, and scattering parameter of the RF interaction cavity, the structure is simulated using CST's eigenmode solver, and frequency-domain solver, respectively.

4.5.1.1. Results of Eigenmode Solver

To know the EM behavior of the RF interaction cavity of the reltron, the structure is designed according to the structural specification listed in Table 4.2. The geometry of the RF interaction cavity (i.e. SCC) consists of the main pillbox cavity, coupled-cavity, and three metal discs. These metal discs are placed at the front, middle, and end of the main pillbox cavity. The metal disc placed in the middle splits the main pillbox cavity into two identical sections called front and back main pillbox cavities, respectively, as shown in Fig. 4.1 (b). This multi-cavity RF interaction cavity is designed and simulated with the help of an eigenmode solver and the obtained results are shown in Fig. 4.4. From the figure, the electric field distribution associated with different resonating modes of the RF interaction cavity and their respective resonant frequency can be seen. From Fig. 4.4 (a), it is seen that for 0-mode, the electric field in the adjacent main pillbox cavities are in the same phase and the phase difference between the electric field present in the coupled cavity and the main pillbox cavities is zero, while in the case of π-mode (i.e. Fig. 4.4 (c)), the electric field in the adjacent main cavities is in the same phase but the phase difference between the electric field present in the coupled cavity and the main pillbox cavities is 180^{o} (i.e. out of phase). Fig. 4.4 (b) shows the electric field distribution for the $\pi/2$-mode, where the electric field in the coupled cavity is almost zero while the magnitude of the electric field present in the adjacent main pillbox cavities is equal, but the phase difference between them is 180^{o}. The eigenmode solver predicts that the resonating frequency associated with the 0-mode, $\pi/2$-mode, and π-mode is 2.732, 2.866, and 2.952 GHz, respectively.

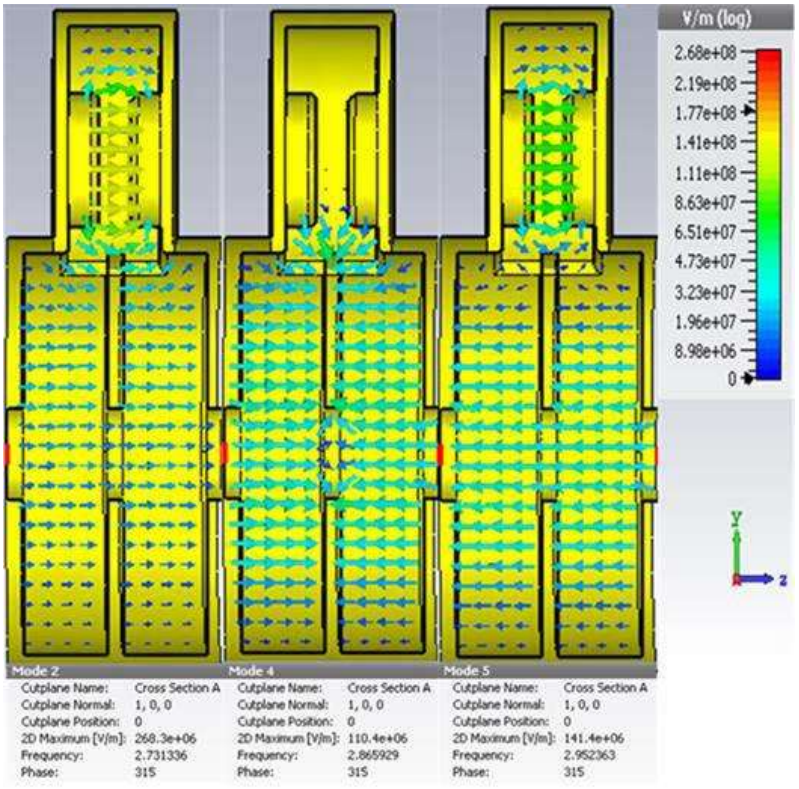

Figure 4.4: The electric field distribution in the RF interaction cavity (electron beam absent) of the reltron with their respective resonant frequency for different operating modes: (a) 0-mode, (b) π/2-mode, and (c) π-mode.

4.5.1.2. Results of Frequency Domain Solver

To ensure the resonating frequency associated with the different resonating modes of the RF interaction cavity the scattering parameters have been obtained. The model of the RF interaction cavity is designed with two axial pins that are connected at the starting and ending position of the front and back main pillbox cavities. To excite these axial pins, a separate waveguide port is used. Now this modeled structure is simulated with the help of a frequency-domain solver. Fig. 4.5 shows the obtained scattering parameter (i.e. S_{11}) of the RF interaction cavity, and from Fig. 4.5, it can be observed that there are three dips.

Each dip of the S_{11} parameter shows the resonating mode of the RF interaction cavity. The marker associated with these dips shows the resonating frequency associated with these modes. The resonating frequency is 2.757, 2.865, and 2.957 GHz, which is close to the resonant frequency predicted by the eigenmode solver.

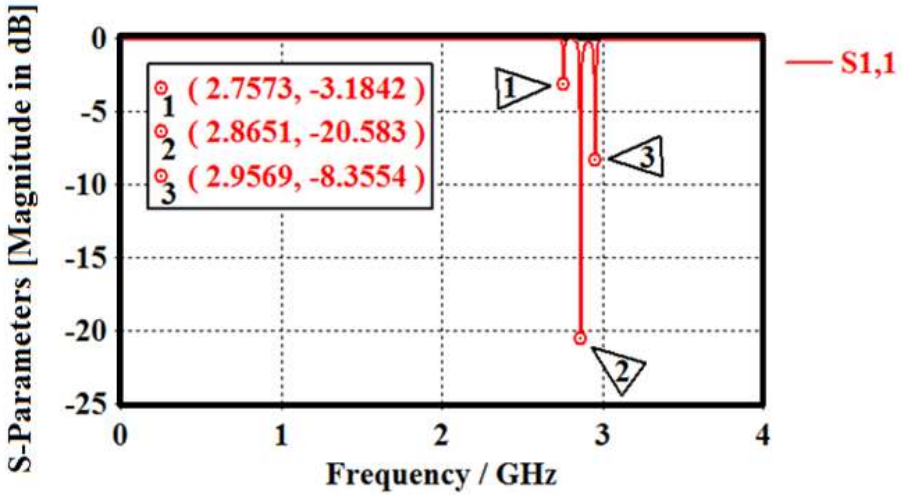

Figure 4.5: Magnitude of the scattering parameter (S_{11}) versus frequency plot of the RF interaction cavity of the reltron.

4.5.1.3. SCC's Structural Parametric Analysis

The effect of various structural parameters of the RF interaction cavity on the resonating frequency associated with the different resonant modes is studied and shown in Fig. 4.6. The effect of variation in the hole radius on the resonating frequency associated with the different modes is shown in Fig. 4.6 (a). It is seen from Fig. 4.6 (a) that with the increase in the hole radius, the resonating frequency associated with π/2-mode increases with a significant amount (this increase in resonating frequency occurred due to an increase in electrical coupling which exists between the adjacent main pillbox cavities), whereas the resonating frequency associated with 0-mode increases with a negligible amount, while for

the π-mode, it increases with a small amount.

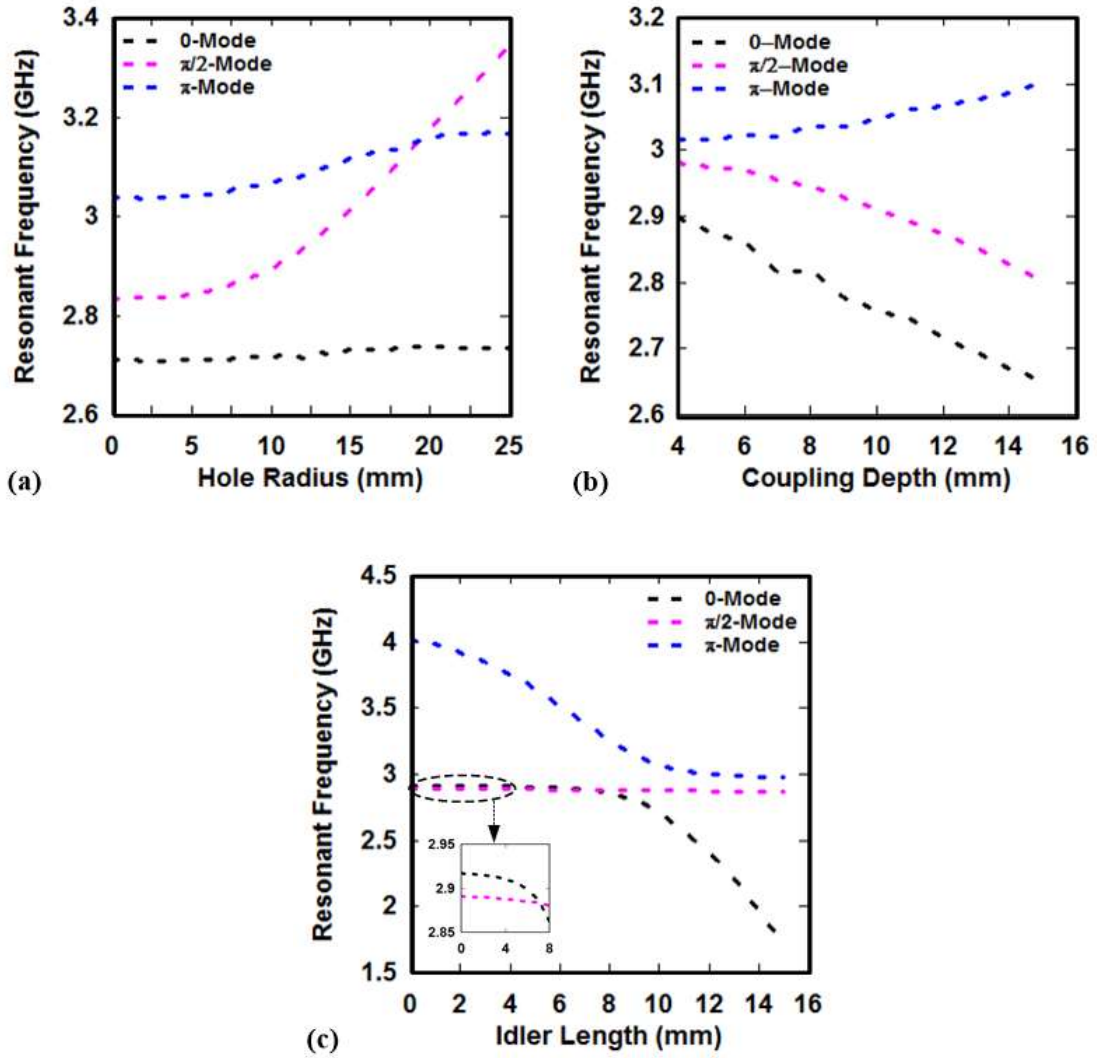

Figure 4.6: The effect of different structural parameters of the RF interaction cavity on the resonating frequency of three different modes: (a) effect of hole radius, (b) effect of coupling depth, and (c) effect of idler length.

The effect of the magnetic coupling depth on the resonating frequency associated with the various resonant modes is shown in Fig. 4.6 (b). From Fig. 4.6 (b), it is seen that with the increase in the coupling depth (i.e. the coupling slot area (A_s) increases), the resonating frequency associated with 0-mode and π/2-mode is decreased, whereas the resonating

frequency of π-mode increases. Fig. 4.6 (c) shows the effect of the idler length on the resonating frequency. From Fig. 4.6 (c), it is seen that the resonating frequency of the π/2-mode is independent of the variation of idler length, while with the increment in the idler length, the resonating frequency is associated with the 0-mode and π-mode get reduced significantly.

4.5.2. Hot Test Simulation Results

A typical modeled grid-less reltron oscillator is designed and simulated with the help of a CST's PIC solver. The typical beam parameters selected for the PIC simulation are taken from the experimental reported work on the grid-less reltron and are listed in Table 4.1. The DC emissive cathode model available in CST is chosen for the electron beam generation. In this model, the beam current of 200 A was applied with an initial kinetic energy of 100 keV, which is equal to the 100 kV DC supply. The high-voltage DC step pulse has been selected as an excitation signal with a rise time of 10 ns and a duration of 5000 ns. This high voltage DC step pulse was applied at the post-acceleration region with the help of the inbuilt function of CST i.e. discrete port.

By selecting some other inbuilt monitor functions such as phase space monitor, waveguide port, the PIC simulation was carried out for 5000 ns. The kinetic energy distribution of the electrons with respect to the axial position is recorded by the phase space monitor at the user-defined interval of time. The RF signal generated inside the extraction cavity of the device is recorded with the help of a waveguide port. The kinetic energy distribution of the electron beam which is recorded by the phase space monitor is shown in Fig. 4.7.

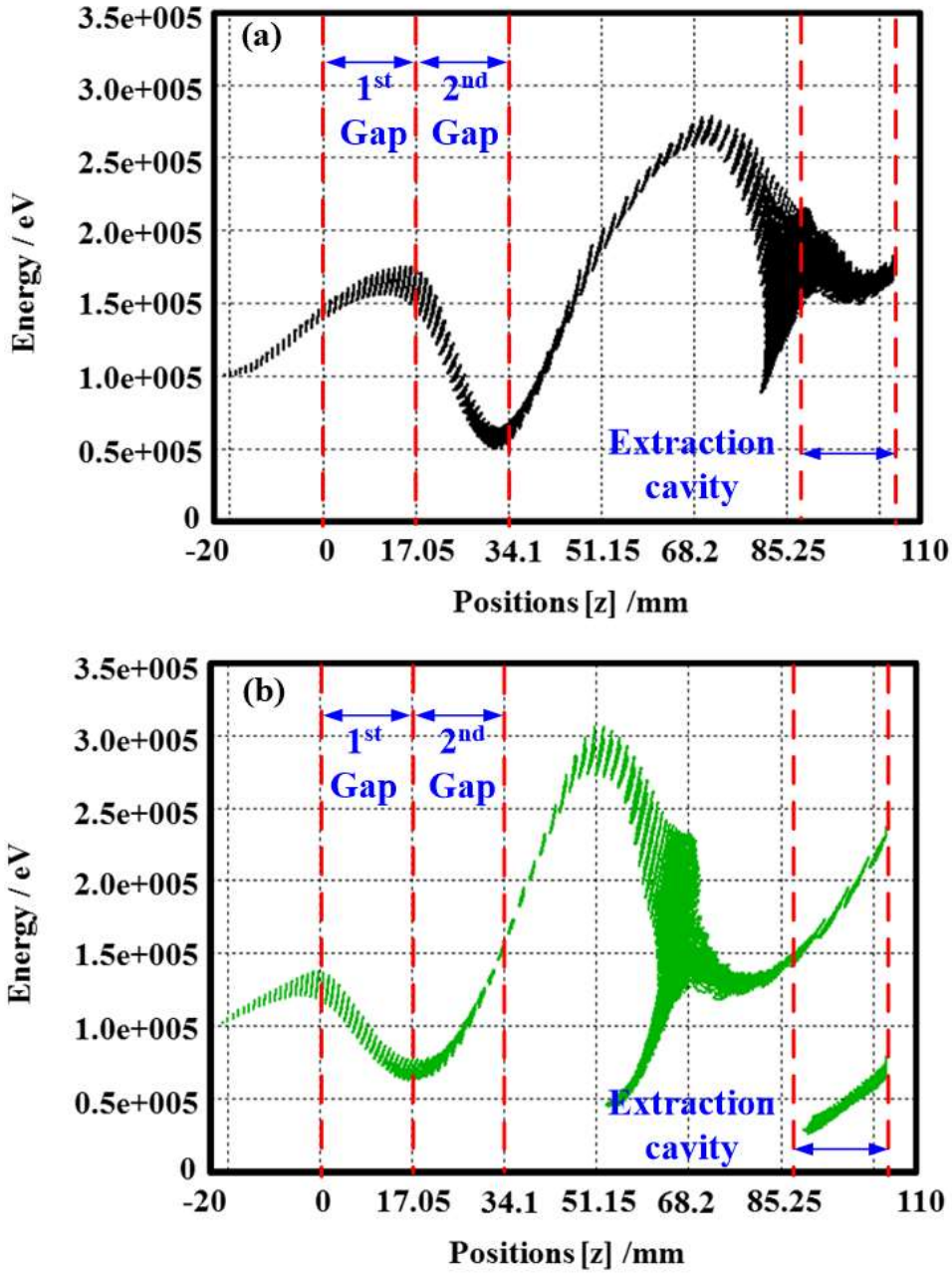

Figure 4.7: Kinetic energy distribution of the electrons: (a) during the first half of the RF cycle and (b) during the second half of the RF cycle of the designed reltron device.

From Fig. 4.7, it is observed that the kinetic energy of the electrons increases in the anode-cathode section very rapidly. Fig. 4.7 (a) and (b) show the kinetic energy distribution of electrons during the first half and the second half of the RF cycle, respectively. During

the first half of the RF cycle, electrons get accelerated in the front main pillbox cavity, while decelerated in the back main pillbox cavity, while during the second half of the RF cycle, due to the reverse Lorentz force, the electron gets decelerated in the front main pillbox cavity and then accelerated in the back main pillbox cavity.

For each half RF cycle, the process of both acceleration and deceleration occurred simultaneously in the RF interaction cavity**,** which leads to the double velocity modulation of the electrons. This process of double velocity modulation not only helps in the formation of intense electron bunches but also introduces an electron's energy spread [Miller *et al.* (1994)]. Fig. 4.8 shows the growth of the RF signal (i.e. electric field) recorded by the waveguide port, which is placed at the extraction cavity. The frequency spectrum of the generated RF signal is shown in Fig. 4.9, which shows that the operating frequency of the modeled grid-less reltron is 2.856 GHz. It is noticed that the operating frequency is ~10 MHz lower than the resonant frequency predicted by the eigenmode solver. This decrease in the operating frequency is observed due to the phenomenon called a beam loading effect.

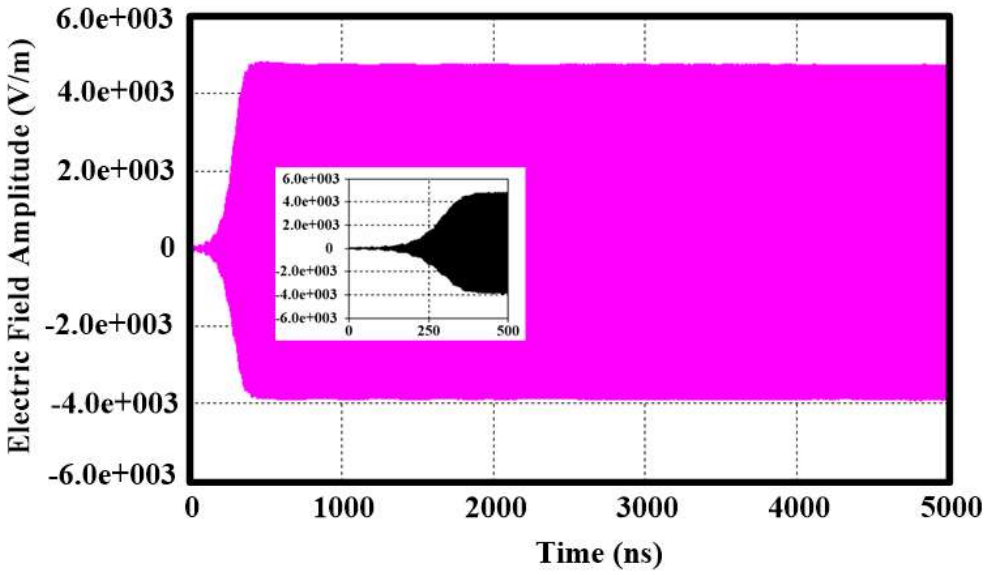

Figure 4.8: Growth of the RF signal recorded at the waveguide port at the extraction cavity.

The typical beam parameter selected here is taken from Table 4.1, i.e. with the initial beam current of 200 A and the total tube voltage of 250 kV, in which 100 kV is applied at the cathode region and the rest 150 kV is applied at the post-acceleration region. With these selected electrical parameters, the PIC simulation shows that the device generates ~22 MW RF output power which is shown in Fig. 4.10. The simulated beam conversion efficiency achieved by the modeled grid-less reltron is 44%.

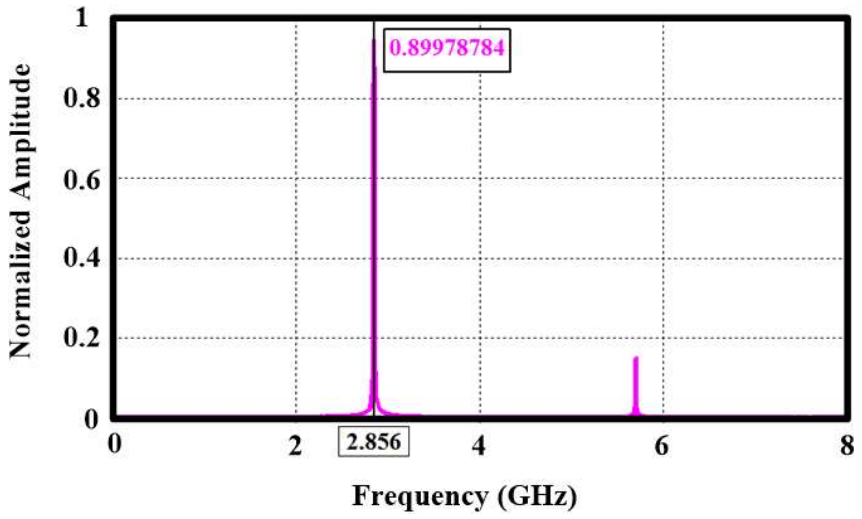

Figure 4.9: Normalized frequency spectrum of the generated RF signal.

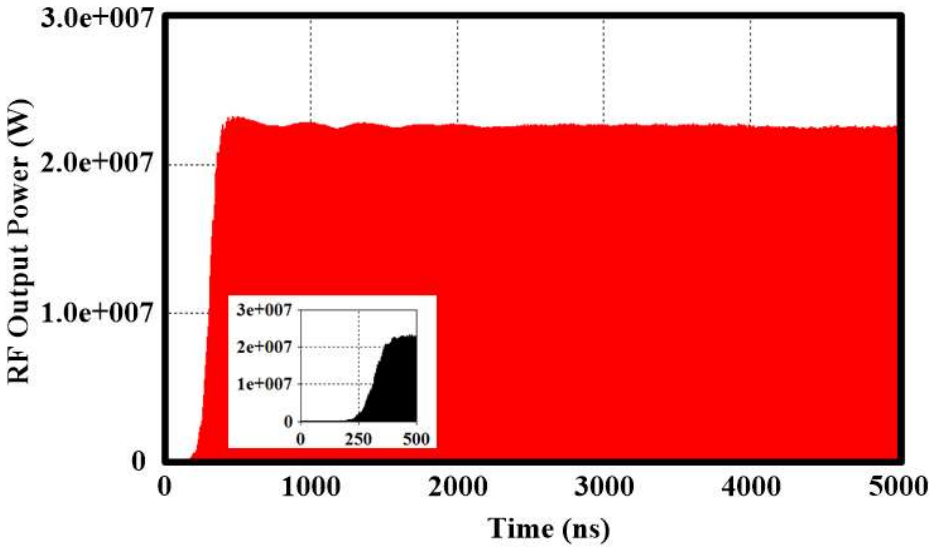

Figure 4.10: RF output power at the extraction cavity.

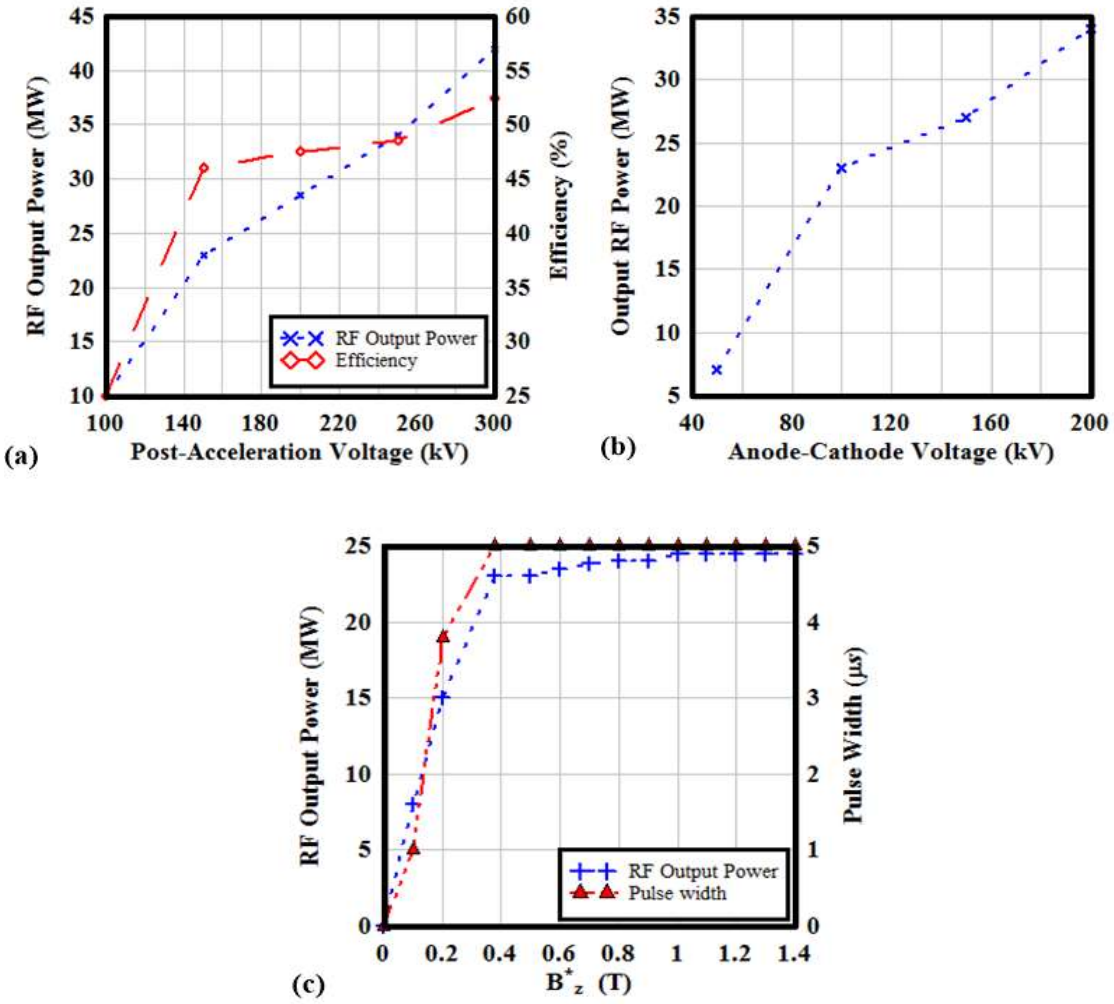

Figure 4.11: Effect of various electrical parameters on the RF output power of the grid-less reltron, due to variation in (a) post-acceleration voltage, (b) anode-cathode voltage, and (c) applied external DC magnetic field.

4.5.2.1. Electrical Parametric Analysis

The RF behavior of the device has been investigated for the various electrical parameters. With the assumption that at a time single electrical parameter is varied consecutively, and the rest parameter is kept constant. The effect of various electrical parameters is shown in Fig. 4.11. From Fig. 4.11 (a), it is seen that with the increase of post-acceleration voltage, the device generates more RF output power, and thus the increase in the device efficiency

is observed. This increment in RF output power is obtained due to the relative kinetic energy spread between the electron bunches gets reduced to a great extent [Miller *et al.* (1992)]. Fig. 4.11 (b), shows the effect of cathode voltage. From the figure, it is seen that with the increase of the cathode voltage, the device produces more RF output power. This increase in the RF output power is due to the increase in the anode-cathode voltage which increases the initial kinetic energy of the electron beam. Finally, Fig. 4.11 (c) shows the effect of the external DC magnetic field on the generated RF output power and its pulse width. Initially, when the applied external DC magnetic field strength is not sufficient to guide the electron beam, high beam divergence has occurred, and therefore, the reduction in RF output power is observed. Also from Fig. 4.11 (c), it is evident that a small external DC magnetic field around 0.4 Tesla is sufficient for guiding the electrons.

4.6. Conclusion

Conventionally reltron uses high-density electrons emitted through explosive emission cathodes which produce high-density plasma inside the device which is responsible for the pulse shortening and also limits the PRR of the device. This problem can be avoided using the thermionic emission cathode in the reltron oscillator i.e. grid-less reltron. In this case, the plasma density is lower due to lower current and remains in its super-conducting zone. Hence longer pulse operation with a higher PRR becomes feasible. The design methodology of the grid-less reltron, the effect of different structural parameters of the RF interaction cavity on the fundamental resonance mode frequency, and finally, the effect of the different electrical parameters on the device performance has been presented. To validate the developed design methodology, the designed grid-less reltron has been compared with the experimental reported device. The simulation results found that the

designed device generates ~22 MW RF output power at the operating frequency of 2.856 GHz with a device efficiency of ~44%. The obtained simulated results have been found within 5% of the experimental values. It is hoped that the design methodology and simulation studies of the grid-less reltron should be useful for the HPM system designers which are looking for higher RF energy, longer RF pulse with high PRR HPM source.